

Bond-selective photofragmentation of jet-cooled HOD at 193 nm: Vibrationally mediated photochemistry with zero-point excitation

David F. Plusquellic, Ondrej Votava, and David J. Nesbitt

Citation: *The Journal of Chemical Physics* **109**, 6631 (1998); doi: 10.1063/1.477314

View online: <http://dx.doi.org/10.1063/1.477314>

View Table of Contents: <http://scitation.aip.org/content/aip/journal/jcp/109/16?ver=pdfcov>

Published by the [AIP Publishing](#)

Articles you may be interested in

Selective bond breaking mediated by state specific vibrational excitation in model HOD molecule through optimized femtosecond IR pulse: A simulated annealing based approach

J. Chem. Phys. **139**, 034310 (2013); 10.1063/1.4813127

H⁺ versus D⁺ transfer from HOD⁺ to CO₂: Bond-selective chemistry and the anomalous effect of bending excitation

J. Chem. Phys. **134**, 064312 (2011); 10.1063/1.3534908

Dissociation dynamics of thiolactic acid at 193 nm: Detection of the nascent OH product by laser-induced fluorescence

J. Chem. Phys. **120**, 6964 (2004); 10.1063/1.1667878

Photodissociation dynamics of jet-cooled H₂O and D₂O in the non-Franck–Condon regime: Relative absorption cross sections and product state distributions at 193 nm

J. Chem. Phys. **107**, 6123 (1997); 10.1063/1.474280

Photofragment excitation spectrum for O(1D) from the photodissociation of jet-cooled ozone in the wavelength range 305–329 nm

J. Chem. Phys. **106**, 6390 (1997); 10.1063/1.473629



Bond-selective photofragmentation of jet-cooled HOD at 193 nm: Vibrationally mediated photochemistry with zero-point excitation

David F. Plusquellic

Optical Technology Division, National Institute of Standards and Technology, Gaithersburg, Maryland 20899

Ondrej Votava and David J. Nesbitt^{a)}

JILA, National Institute of Standards and Technology, University of Colorado, Campus Box 440, Boulder, Colorado 80309-0440 and Department of Chemistry and Biochemistry, University of Colorado, Boulder, Colorado 80309

(Received 27 April 1998; accepted 23 July 1998)

Photofragment yields are reported for supersonically cooled H₂O, D₂O, and HOD via one photon, 193 nm photolysis in a slit jet expansion, with OH and OD fragments monitored by laser induced fluorescence methods. Detailed analysis of the dependence of OH vs OD photofragment signals on isotopic composition is used to extract relative photolysis cross sections and branching ratios for bond-selective cleavage in HOD, H₂O, and D₂O samples. Specified relative to the 193 nm cross sections for H₂O→H+OH, the ratios are 0.392(20), 0.032(20), and 0.0157(19) for (i) HOD→H+OD, (ii) HOD→D+OH and D₂O→D+OD channels, respectively. Specifically, these results indicate a propensity for H–OD vs D–OH bond cleavage in HOD of 12(8):1. This strong H/D isotopic selectivity reflects extreme non-Franck–Condon photolysis out of classically of forbidden regions of the ground-state wave function, i.e., bond-selective photochemistry mediated solely by zero-point vibrational excitation. However, when compared with theoretical predictions from full three-dimensional quantum scattering calculations on the ground (\tilde{X}^1A_1) and excited (\tilde{A}^1B_1) potential-energy surfaces (PES) of water, the observed HOD branching ratio is found to be *too low* by an order of magnitude. These results provide additional evidence that photodissociation of water in the extreme non-Franck–Condon region is not adequately explained by current theoretical models and suggest that contributions from other electronic surfaces may be important.

© 1998 American Institute of Physics. [S0021-9606(98)01140-4]

I. INTRODUCTION

In recent years, methods of studying unimolecular photofragmentation processes have matured from one photon, direct absorption techniques toward multiresonance photodissociation schemes in an effort to achieve control of the fragmentation dynamics toward a specific target channel. In conventional vibrationally mediated photodissociation (VMP) methods, the first [infrared (IR) pump] photon is used to prepare the reagent in a specific rovibrational wave function, which in turn permits a second [ultraviolet (UV) photolysis] photon to selectively dissociate this state via absorption from favorable Franck–Condon regions. As one logical extreme of this approach, strict control of the fragmentation pathway may be achieved by choosing sufficiently low photolysis energies to preferentially excite molecules in the classically forbidden, Gaussian “tails” of the vibrational wave function, and thereby, in principle, obtaining exponential selectivity for fragmentation into a particular branching ratio.

Asymmetric triatomic molecules have been attractive candidates for such studies since two distinguishable atom + diatom fragmentation pathways exist over a relatively wide range of photolysis energies. In particular, HOD has been a

long-time favorite target for both experimental and theoretical studies because of its small size, the convenient access to vibrational modes having mostly OH or OD stretch character, and the simplicity of its electronic state structure. One goal has been to manipulate the H–OD to D–OH branching ratio through intermediate vibrational state selection prior to photodissociation on the purely repulsive \tilde{A} surface. From many such studies, the OD vs OH yields have been found to depend strongly both on the vibrational state character and the wavelength of photolysis photon. For example, the fundamental ($\Delta v = 1$) stretch modes of HOD have been excited by stimulated Raman excitation (SRE), followed by photodissociation at 193 nm and laser induced fluorescence (LIF) detection of the OH and OD products. A clear 2.5-fold enhancement of OD vs OH formation is observed for $\nu_{OH} = 1$ excitation of the HOD target, whereas $\sim 1:1$ OH and OD yields are found for $\nu_{OD} = 1$ excitation.¹ Greater mode selectivity is predicted² and observed from higher overtone vibrational levels in HOD. For example, Crim and co-workers³ report a 15-fold enhancement of OD over OH for dissociation of $4\nu_{OH}$ excited HOD at both 240 and 266 nm. Most recently, Brouard and Langford⁴ have observed OD/OH ratios in excess of 12:1 and 23:1 from the $4\nu_{OH}$ and $5\nu_{OH}$ levels, respectively, for dissociation of HOD at 288 nm.

Bond-breaking selectivity is anticipated to be less pro-

^{a)}Staff member, Quantum Physics Division, National Institute of Standards and Technology. Electronic mail: reception.desk@jila.colorado.edu

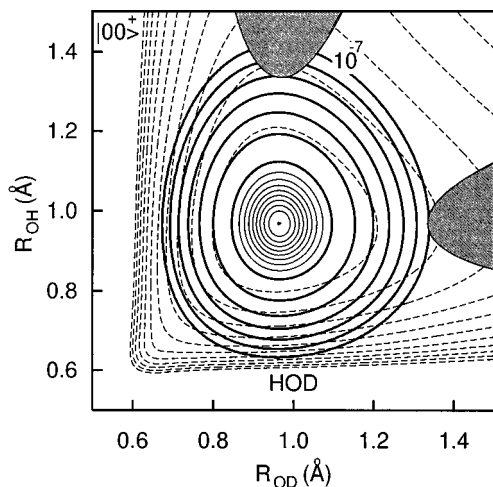


FIG. 1. Contour plots of the Sorbie–Murrell ground-state potential-energy surface (dashed lines at 1 eV spacing) and the square modulus (solid lines) of the zero-point vibrational wave function of HOD along the two stretch coordinates at fixed bond angles of 104.5° . Also shown in gray are regions on the Staemmler and Palma excited state PES energetically accessible at wavelengths ≥ 193 nm relative to zero-point level. The probabilities are shown on two different grid spacings in order to illustrate the far-off resonance absorption region at 193 nm. The lighter contours decrease linearly from a peak value of 1 to 0.1 in 0.1 unit intervals; the heavier contours represent tenfold sequential decreases from 10^{-1} to 10^{-7} .

ounced for total energies that sample the barrier region for crossing between the D+OH and H+OD product channels on the excited state surface. This has been experimentally verified for direct one-photon dissociation of HOD at 157 nm, where only a $4 \pm 1:1$ ratio of OD to OH is observed.⁵ Most relevant in this regard are the VMP studies of the $4\nu_{\text{OH}}$ level of HOD, where 218 nm yields in the OD and OH channels are found to be nearly identical despite 12:1 enhancements observed at 288 nm.³ These mode-selective trends are reasonably well understood both for excitations above and below the barrier, with current theoretical models in good qualitative agreement with the observed dynamics.⁶ For total energies below the barrier, the enhancement of OD vs OH product yields by ν_{OH} excitation takes advantage of red-shifted but classically allowed excitations from extended OH bond geometries that characterize the intermediate vibrational state. Conversely, selectivity for the H+OD channel becomes increasingly dominant below the barrier due to increasingly weaker Franck–Condon overlap onto the D+OH channel.

Similarly, H–OD vs D–OH bond cleavage should also be strongly favored for Franck–Condon excitations in the classically forbidden region, but now with an exponential sensitivity of this branching ratio on the photolysis energy. This is particularly evident at 193 nm for zero-point excitation of HOD where full three-dimensional (3D) quantum mechanical scattering calculations run on the Sorbie–Murrell⁷ (SM) and Staemmler–Palma⁹ (SP) PES predict a more than 100:1 selectivity for OD vs OH product.⁹ Figure 1 provides a simple interpretation of these theoretical findings. Contour plots of the 2D (two-dimensional) ground-state wave function probabilities of HOD along the OH and OD stretch coordinates are superimposed on the SM PES for a fixed HOD

bond angle of 104.5° . The regions on the SP surface vertically accessible at 193 nm are illustrated with shaded region along both the OH and OD stretch coordinates. In a zeroth-order picture, the absorption cross sections are dominated by the small Franck–Condon overlap regions between probability densities associated with (i) the continuum state (which peaks near the classical turning point) and (ii) exponentially decreasing ground-state wave functions. Thus, a $\approx 100:1$ branching ratio for OD to OH formation may be estimated from the ratio of the maximum wave function probability at the points of intersection with the SP PES, in good agreement with quantum scattering theory. As will be demonstrated in this study, however, the experimentally observed OD/OH branching ratios are far smaller, theoretically overestimated by more than eightfold. In conjunction with the $>$ threefold differences between calculated and observed absorption cross section ratios for H₂O and D₂O noted previously,¹⁰ these discrepancies provide supporting evidence that current theoretical models are inadequate for characterizing photofragmentation dynamics initiated from classically forbidden regions of water.

Our interest in studies of OH/OD photofragment product yields of HOD at 193 nm rises from several sources. First, in contrast with the previous studies of H₂O and D₂O, the branching ratio for photofragmentation of jet-cooled HOD involves a single rovibrational wave function with two experimentally distinguishable products. The observed dynamics for this bond fission process, therefore, provide rigorous additional tests of the potential-energy surfaces and scattering theory for water in non-Franck–Condon absorption regions. Second, while in principle the absorption cross section ratio of H₂O and D₂O should be obtainable directly from the product yields from photolysis of pure samples, in practice some level of contamination of D₂O with HOD is unavoidable. Therefore, the trends observed from analysis of isotopic mixture provide a quantitative way to extrapolate to the limit of pure H₂O, D₂O, and HOD samples for accurate determinations of bond-selective product yields.

The remainder of this paper is organized as follows. In Sec. II, we provide a brief review of the experimental apparatus and the methods used to obtain the OH and OD photofragment populations from the experimentally measured laser induced fluorescence (LIF) intensities. The equilibrium expressions and liquid–vapor phase properties of the H₂O, D₂O, and HOD isotopomers that dictate sample compositions are discussed in Sec. III. In Sec. IV, the OH/OD photofragment yields are determined for a compositional series of photolyzed samples and fit to expressions to obtain the branching ratios and relative absorption cross sections. The OD product state distributions, Λ -doublet and spin-state ratios inferred for “pure” HOD samples are compared with those previously reported for 193 nm photolysis of H₂O and D₂O.¹⁰ In Sec. V, predictions based on a semiclassical Condon model of the dissociation serve to test the sensitivity of OD/OH branching ratios for HOD to uncertainties in the upper–lower potential-energy surfaces. The paper is summarized in Sec. VI.

II. EXPERIMENT

The experimental apparatus for far off resonance photo-dissociation studies of jet-cooled H₂O–HOD–D₂O and LIF detection of the OH/OD photofragments has been reported elsewhere in detail¹⁰ and is briefly summarized below. Gas mixtures of 1% H₂O–D₂O–HOD in He are expanded through a 4 cm×50 μm slit jet at 340 Torr into a vacuum chamber. Both the 193 nm photolysis (ArF excimer, unstable resonator optics) and 308 nm probe (frequency doubled R6G) lasers intersect the supersonic expansion, parallel to the slit axis and 1.25 cm downstream from the nozzle orifice. The resulting OH/OD photofragments are probed on $\tilde{A}^2\Sigma^+(v'=0) \leftarrow \tilde{X}^2\Pi(v''=0)$ electronic transitions after a 200 ns delay following the photolysis pulse. Laser induced fluorescence is monitored with a high efficiency (≈5%) light collection assembly optimized for the slit jet geometry, which also provides convenient spatial filtering of probe and photolysis laser light with a greater than 10⁹ rejection ratio. This combination of (i) slit jet path length and (ii) high sensitivity LIF detection results in photolysis cross-section detection limits as low as ≈10⁻²⁶ cm², which is what make such far-off resonance photodissociation studies experimentally feasible.

Rotational and fine structure state populations are obtained from the integrated LIF signals based on the following model, which takes partial optical saturation of the OH and OD transitions into account. Each population, $n(v'',J'')$, is determined from the integrated LIF intensities, S , via

$$S \propto Bn(v'',J'')I_{\text{probe}}m_1/(1+m_2I_{\text{probe}}), \quad (1)$$

where B is the Einstein coefficient for absorption,¹¹ I_{probe} is the probe laser pulse energy and the parameters m_1 and m_2 reflect LIF detection efficiency and optical saturation, respectively. The relevant experimental parameters for all OH/OD transitions have been reported elsewhere.¹⁰ By way of a consistency check, typical populations obtained from both P - and R - branch lines agree to better than 10%. This is particularly important in the present mixed isotope studies since the OH/OD (0,0) spectral bands are strongly overlapping and thus the populations can often solely be determined from only one component of the P/R pair. No vibrationally excited products are observed for the 193 nm photolysis of HOD; signal to noise on the $v=0$ species establishes an upper limit on the $v=1/v=0$ ratio of <0.5%. Data analysis on the $\Pi_{1/2}^-$ state populations is limited by multiply unresolved Q -branch rotational transitions in the LIF spectrum. Effective OH or OD product yields are, therefore, obtained by summing over all N for each of the three other $\Pi_{3/2}^+$, $\Pi_{3/2}^-$, and $\Pi_{1/2}^+$ fine structure states.

III. LIQUID AND GAS-PHASE ISOTOPIC SAMPLE COMPOSITIONS

The gas-phase isotopic compositions used in the determination of the bond-selective cross sections of H₂O, D₂O, and HOD depend on (i) the liquid phase equilibrium compositions used to prepare the gas samples and (ii) the temperature-dependent vapor pressures above the premixed liquid samples. The liquid samples are prepared from pipet-

TABLE I. Initial D₂O liquid phase compositions, $\chi_{\text{D}_2\text{O}}^0$, final gas-phase equilibrium mole fraction compositions, χ^g , from Eq. (3) and the % OH and % OD product yields obtained for the 193 nm photolysis of jet-cooled H₂O, D₂O, and HOD samples. The OH and OD product yields are normalized to 100% for photolysis of pure H₂O. These measurements are repeated between 3–9 times for each isotopic composition; 1 σ error bars represent the standard deviation of the mean.

$\chi_{\text{D}_2\text{O}}^0$	$\chi_{\text{H}_2\text{O}}^g$ ^a	$\chi_{\text{D}_2\text{O}}^g$ ^a	χ_{HOD}^g ^a	% OH	% OD
0.00	1.00	0.00	0.00	100(6)	0.0(2)
0.25	0.58	0.059	0.36	59(4)	15.2(12)
0.50	0.27	0.24	0.49	30(2)	20.8(12)
0.75	0.072	0.55	0.38	8.2(4)	15.6(6)
0.90	0.012	0.80	0.19	2.7(5)	9.5(10)
0.998 ^b	0.00	0.995 ^c	0.005 ^c	0.0(2)	1.77(33)

^aEstimated uncertainties of the gas-phase compositions delivered by the slit jet are ±1%.

^bPurity obtained from NMR studies of the % H atom concentration in the liquid samples.

^cPurity determined by LIF detection of OH and OD products following multiple purge cycles of the gas delivery system. See text for details.

ted aliquots of H₂O and D₂O, shaken to ensure complete mixing and rapid H/D isotopic exchange. The D₂O isotopic purity is confirmed by nuclear magnetic resonance (NMR) tests to be at the stated 99.8 D atom % level; particular care is taken to passivate surfaces by multiple contact with solutions prior to making final mixes. Uncertainty in the initial liquid phase H₂O/D₂O mole fractions is estimated to be less than 1%. From stoichiometry, the isotopic equilibration can be expressed in terms of the initial mole fractions of H₂O and D₂O liquids, $\chi_{\text{H}_2\text{O}}^0$, and the equilibrium mole fraction of HOD, χ_{HOD}^g , i.e.,



$$K_{\text{eq}}^g = (\chi_{\text{HOD}}^g)^2 / [(\chi_{\text{D}_2\text{O}}^0 - 0.5\chi_{\text{HOD}}^g) \cdot (\chi_{\text{H}_2\text{O}}^0 - 0.5\chi_{\text{HOD}}^g)], \quad (3)$$

where the experimentally measured equilibrium constant¹² for H/D isotope exchange is 3.74±0.02 at 25 °C. Equation (3) can be solved for the equilibrium mole fraction of HOD (χ_{HOD}^g), which by the stoichiometry in Eq. (2) yields the liquid phase mole fractions (χ_{HOD}^0 and $\chi_{\text{D}_2\text{O}}^0$) of the H₂O and D₂O isotopomers.

Due to small differences in vapor pressures for the three different isotopomers, the gas-phase composition will differ subtly from the liquid phase mole fractions obtained from Eq. (3). To take this into account, the known equilibrium vapor pressures¹³ of H₂O, D₂O, and HOD at 25 °C are used via Henry's Law to predict the relative partial pressures and, therefore, gas-phase mole fractions of the three isotopomers evaporating from the liquid sample. In these determinations, the mixed solutions of H₂O, D₂O, and HOD are assumed to be ideal; partial pressure deviations¹⁴ from this limit are less than 0.2% and well within the uncertainties reported herein. The resulting mole fraction compositions are listed in Table I and graphically displayed in Fig. 2 as a function of initial liquid phase composition of D₂O, $\chi_{\text{D}_2\text{O}}^0$. The gas samples are then prepared by evaporation of the liquid samples into an evacuated stainless steel mixing tank at 25 °C, which has

GAS PHASE ISOTOPIC COMPOSITIONS

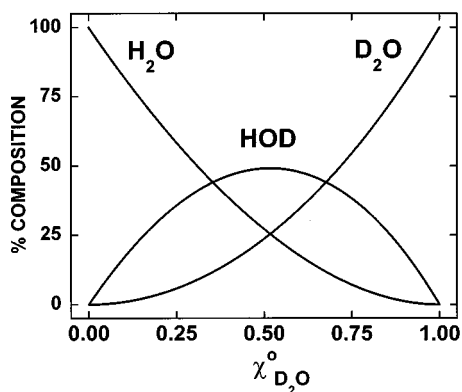


FIG. 2. Percentage of H_2O , D_2O , and HOD in the gas samples as a function of the initial liquid composition of D_2O . The gas-phase compositions are determined from the partial pressures of the liquid phase components at 25°C using Henry's Law with specific corrections made for the differences in the vapor pressures (Ref. 14) for H_2O , D_2O , and HOD using $P_{\text{H}_2\text{O}}/P_{\text{D}_2\text{O}}=1.145$ and $P_{\text{H}_2\text{O}}/P_{\text{D}_2\text{O}}=(P_{\text{HOD}}/P_{\text{D}_2\text{O}})^{1/2}$. The latter condition is exact for ideal solution behavior, which is known from previous studies to be a reliable approximation (Ref. 14).

been pre-passivated by multiple exposures with the target isotopic composition before a final fill and dilution with He to yield 1% mixtures.

As a final note, if left unchecked, the liquid sample can evaporatively cool by several degrees while filling the stainless steel mixing tank, which can in principle influence the sample isotopic composition by either a temperature-dependent change in (i) liquid phase equilibrium constant or (ii) isotopic vapor pressure ratios. The former effect is less than 1% for $\Delta T \approx 25^\circ\text{C}$ and, therefore, negligible ($K_{\text{eq}}^{\text{H}_2\text{O}} = 3.74$ at 25°C and $K_{\text{eq}}^{\text{D}_2\text{O}} = 3.75$ at 0°C).¹² However, the latter effect on isotopic vapor pressure ratios can be more significant, changing by 2%–7% between 0°C and 25°C .¹³ As a result, the samples are heated mildly during these transfers to compensate for evaporative cooling of the liquid and maintain $T \approx 20$ – 25°C conditions.

Gas sample delivery to the probe–photolysis region requires contact with stainless steel surfaces in the pulsed slit jet expansion valve. For each gas sample, therefore, the slit valve is treated with a series of multiple exposure–evacuation cycles to ensure complete accommodation. This degree of passivation is explicitly quantified by performing photolysis measurements and sampling changes in the experimentally observed OH/OD ratios as a function of the number of gas-phase exposures.¹⁰ Accommodation is found to be essentially complete (>99%) within four passivation cycles, as further tested by comparing the asymptotic OH/OD results starting from both *over-* and *under-*deuterated initial conditions. Based on the multiple checks described above, the net uncertainty in gas-phase isotopic composition delivered to the experimental probe region is estimated to be $\pm 1\%$. This is negligible with respect to the order of magnitude discrepancies between theory and experiment that these photolysis measurements elucidate, as described in more detail below.

IV. RESULTS AND ANALYSIS

A. OH and OD bond selective quantum yields and branching ratios

The relative cross sections for photolysis of individual bonds in H_2O , D_2O , and HOD are obtained from analysis of the OH and OD photofragment yields as a function of fractional gas-phase isotopic composition. The effective cross section for generating OH vs OD population from 193 nm photolysis of an isotopically mixed gas sample may be expressed in terms of bond selective cross sections and gas-phase mole fraction compositions of the isotomers as

$$\sigma^{\text{OH}} = \sigma_{\text{H}_2\text{O}} \cdot \chi_{\text{H}_2\text{O}}^g + \sigma_{\text{D-OH}} \cdot \chi_{\text{HOD}}^g, \quad (4a)$$

$$\sigma^{\text{OD}} = \sigma_{\text{D}_2\text{O}} \cdot \chi_{\text{D}_2\text{O}}^g + \sigma_{\text{H-OD}} \cdot \chi_{\text{HOD}}^g. \quad (4b)$$

In Eq. (4), $\sigma_{\text{D-OH}}$ and $\sigma_{\text{H-OD}}$ are the cross sections for selective HOD cleavage to form $\text{D}+\text{OH}$ and $\text{H}+\text{OD}$, respectively, while $\sigma_{\text{H}_2\text{O}}$ and $\sigma_{\text{D}_2\text{O}}$ reflect the propensity to cleave *either* bond to form $\text{H}+\text{OH}$ or $\text{D}+\text{OD}$. Experimentally, one measures signals proportional to the nascent state OH and OD populations, i.e., n^{OH} and n^{OD} , obtained by summing over all rotational states in the $\Pi_{3/2}^+$, $\Pi_{1/2}^+$, and $\Pi_{3/2}^-$ manifolds with the help of Eq. (1). The ratio of these population sums (i.e., $n^{\text{OD}}/n^{\text{OH}}$) provides a direct measure of the ratio of the effective cross sections (i.e., $\sigma^{\text{OD}}/\sigma^{\text{OH}}$), from which the ratio of bond selective cross sections (e.g., $\sigma_{\text{H-OD}}/\sigma_{\text{H}_2\text{O}}$, $\sigma_{\text{D-OH}}/\sigma_{\text{H}_2\text{O}}$, and $\sigma_{\text{D}_2\text{O}}/\sigma_{\text{H}_2\text{O}}$) can be extracted.

The OH and OD population sums are determined from the integrated line intensities for a series of photolyzed gas samples of varying isotopic composition. Laser induced fluorescent spectra have been obtained in ≥ 3 independent measurements for samples with $\chi_{\text{D}_2\text{O}}^0 = 0.0\%$, 25%, 50%, 75%, 90%, and 99.8%. To better characterize statistical uncertainties for selected isotope mixtures, multiple additional studies have been repeated for $\chi_{\text{D}_2\text{O}}^0 = 0.0\%$, 75%, and 99.8%. Sample portions of the LIF spectra in the R_{21} branch region for these three samples are shown in the top, middle, and bottom panels of Fig. 3, respectively. The gas-phase compositions and the average values of the photofragment populations determined for each of these samples are given in Table I, with the OH values normalized to 100% for pure H_2O isotopic sample composition. Reported errors reflect one standard deviation of the mean.

The data in Table I are included in a linear least-squares fit of Eqs. (4a) and (4b) to obtain the relative bond-selective cross sections for H_2O , D_2O , and HOD . The data are also represented in the upper and lower panels of Fig. 4 together with the predicted curves generated using these parameters. Normalized to $\sigma_{\text{H}_2\text{O}}$, the best fit parameters for $\sigma_{\text{H-OD}}$, $\sigma_{\text{D-OH}}$, and $\sigma_{\text{D}_2\text{O}}$ are 0.392(20): 0.032(20): 0.0157(19), which correspond to the product channels $\text{H}+\text{OD}$, $\text{D}+\text{OH}$, and $\text{D}+\text{OD}$. Consistent with our earlier results,¹⁰ the ratio of photolysis cross sections for H_2O and D_2O , i.e., $\sigma_{\text{H}_2\text{O}}/\sigma_{\text{D}_2\text{O}}$, is determined to be 64(10), where the uncertainty represents one standard deviation. Of specific interest, however, the branching ratio for bond specific photofragmentation of HOD at 193 nm to form OD or OH fragments (i.e.,

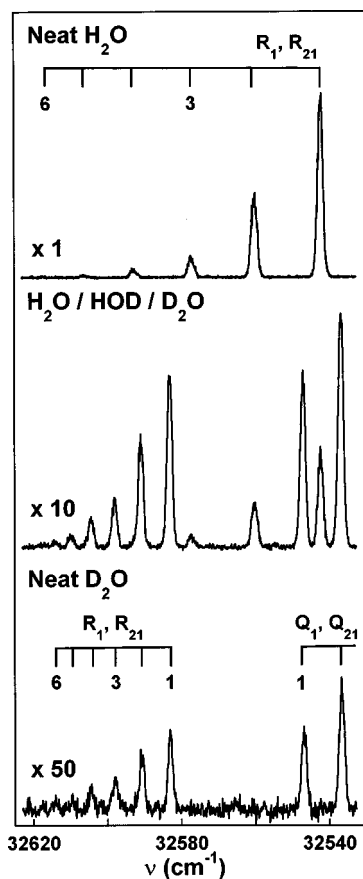


FIG. 3. Example of LIF spectra of OH ($v=0$) and OD ($v=0$) in the R_{21} branch region obtained from 193 nm photolysis of samples with $\chi_{D_2O}^0 = 0\%$ (upper), 75% (middle), and 99.8% (lower). The OD signal in the middle panel is primarily from cleavage of the OH bond in HOD with $<5\%$ originating from photolysis of D_2O . The intensities of the lower two spectra are scaled by 10 and 50 relative to the top panel.

$\sigma_{H-OD}/\sigma_{D-OH}$) is found to be 12(8), where the fractional uncertainty in this ratio represents the fractional uncertainties in each of the photolysis cross sections summed in quadrature. As elucidated in the next section, the most significant source of uncertainty in these determinations is associated with the relative cross section for $D+OH$ bond cleavage in HOD, since this channel is detected via OH formation that competes with the more facile fragmentation of H_2O . Conversely, the relative cross section for $H+OD$ bond cleavage from HOD is well determined in this analysis. As anticipated, the results clearly indicate more facile cleavage of the $H-OD$ vs $D-OH$ bond. However, this ratio is nearly an order of magnitude *smaller* than predicted theoretically; in essence, a surprisingly by large fraction of HOD photolysis at 193 nm occurs via cleavage of the $O-D$ vs $O-H$ bond.

B. OD rotational distributions from 193 nm photolysis of HOD

It is also of dynamical interest to extract the HOD photofragment distributions from these UV photolysis/LIF measurements. Since the OH–OD LIF signals in general arise from photolysis of all three isotopomers, it is first necessary to characterize distributions from 193 nm photolysis of isotopically neat H_2O and D_2O samples, which have been re-

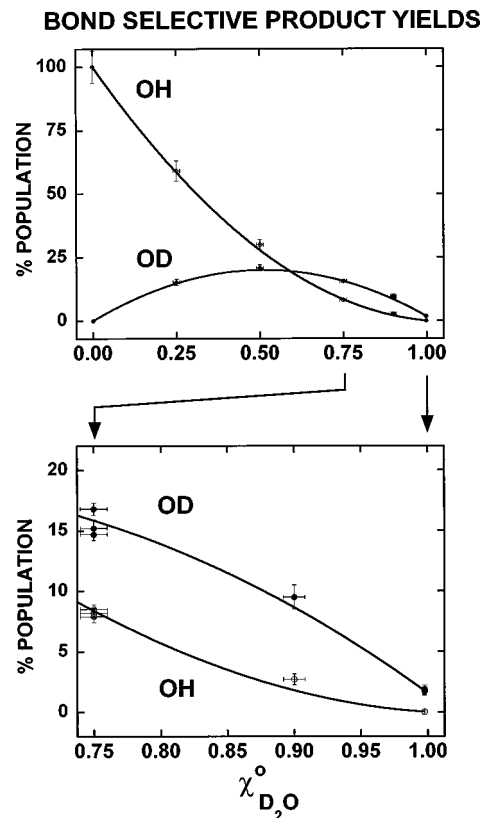


FIG. 4. OH and OD photofragment yields from the 193 nm photolysis of jet-cooled samples as a function of the initial liquid composition of D_2O ($\chi_{D_2O}^0$). The data in the expanded region shown in the lower panel are the most sensitive to determination of the OH–OD branching ratio. Error bars along the abscissa correspond to the maximum uncertainties in the gas-phase compositions associated with the OH and OD yields. Error bars along the ordinate represent one standard deviation of the mean for separate data runs.

ported elsewhere.¹⁰ However, the ease with which the OH/OD photolysis distributions for HOD can be isolated from H_2O and D_2O depends sensitively on the relative magnitude of these additional contributions, which turns out to be much less optimum for OH than for OD products. Specifically, OH production from HOD requires a nominally “unfavorable” cleavage of the OD bond, which must compete with the 30-fold more facile OH bond photolysis of H_2O also present in the mixture. One can effectively increase the HOD– H_2O ratio with excess D_2O , at the expense, however, of absolute HOD concentration. Even at the highest D_2O levels with sufficient S/N to detect OH, the contributions from HOH are comparable to those from HOD photolysis. This makes it unfeasible to extract the one from the other, especially in the presence of the much stronger and partially overlapping OD signals from D_2O .

Fortunately, these trends are exactly reversed for measuring OD product distributions from 193 nm photolysis of HOD. Now the photolysis cross sections are relatively “favorable” since an OH bond is being cleaved, while the competing channel for forming OD from D_2O requires unfavorable cleavage of an OD bond. As a result, the OD signals are dominated by HOD photolysis. This point is evident in Figs. 2 and 4, which demonstrate that the experimentally observed

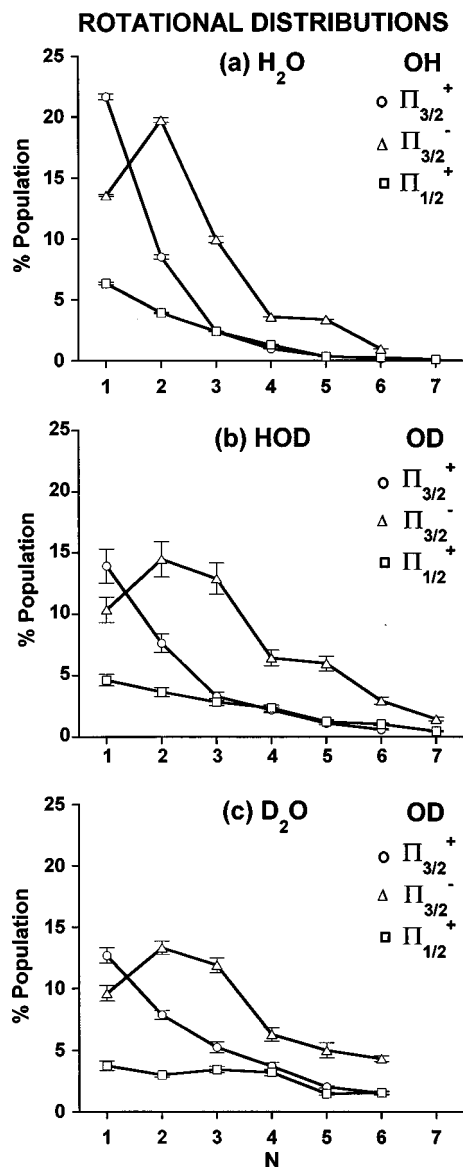


FIG. 5. Rotational state distributions in the $2\Pi_{3/2}^+$ (circles), $2\Pi_{1/2}^+$ (squares), and $2\Pi_{3/2}^-$ (triangles) levels of OH from H_2O (top), of OD from HOD (middle), and of OD from D_2O (lower) following the 193 nm photolysis of jet-cooled samples. The product state yields in each panel are reported so that they sum to 100%. The OD rotational populations from both HOD and D_2O are strikingly similar and reflect significantly broader rotational distributions than observed for OH production from H_2O . These isotopic trends are poorly reproduced from Franck–Condon models and suggest the importance of exit channel torques on OD vs OH products. The error bars reflect 1σ of the mean over 3–9 separate measurements.

OD product closely mirrors the rise and fall of HOD concentrations in the isotopic mixtures. More quantitatively, the contribution to total OD yield from HOD photolysis is 95% for samples with $\chi_{\text{D}_2\text{O}}^0 = 75\%$, which makes it relatively straightforward to correct for the 5% contribution from D_2O photolysis.

The OD photofragment distributions from 193 nm photolysis of HOD are shown in the middle panel of Fig. 5 for the $2\Pi_{3/2}^+$, $2\Pi_{1/2}^+$, and $2\Pi_{3/2}^-$ ground-state levels of OD. For comparison, the 193 nm photofragment distributions from H_2O and D_2O are shown in the upper and lower panels, respectively. The most obvious differences are between the

OH rotational distributions from H_2O that are more sharply peaked at low N and the OD distributions from HOD photolysis that are spread out over a much broader range of N values. One simple contribution to this difference is that the rotational energy spacings in the OH fragment are twice as large as for OD, which for comparable energy deposition into rotation would tend to focus the population into lower N levels. This interpretation would also be supported by the OD rotational distributions from D_2O photolysis, which are overall quite similar to those from HOD.

Alternatively, the Franck–Condon model¹⁵ of Balint–Kurti and Shapiro has been extensively used to interpret product state distributions from H_2O photolysis. This model is based on expressing the ground-state bending wave function as an expansion in free rotor states of the asymptotic diatom+atom product channel. Since this is sensitive only to the Franck–Condon overlap of initial and final state wave functions, this model implicitly neglects all torques in the exit channel between the recoiling product fragments. Despite such approximations, this simple theory has been generally successful in modeling OH distributions from H_2O photolysis.¹⁶ From this perspective, one might rationalize the narrower OH rotational distributions as a result of larger amplitude H_2O vs HOD bending wave functions which, therefore, project onto fewer final rotational channels.

There are several indications in the data, however, that this cannot be the predominant effect. First of all, this same model would also predict even higher OD rotational state populations for D_2O vs HOD photolysis, whereas the observed rotational distributions are in fact quite similar (see Fig. 5). Furthermore, it has been noted in previous studies that initial rotation of water characteristically leads to additional rotation in the OH product. Due to nuclear spin statistics, H_2O can only cool down into a 3:1 population ratio for the 1_{01} and 0_{00} rotational levels. By way of contrast, HOD has no nuclear spin constraints and cools in the slit jet almost completely (>95%) into the 0_{00} level. Similarly, D_2O has an inverted 2:1 nuclear spin preference, and thus has two-thirds of the population in the 0_{00} rotational state. If anything, therefore, the effect of initial rotation would contribute to warmer distributions for H_2O vs HOD or D_2O , whereas the opposite is observed. Indeed, despite considerable effects to characterize populations for 193 nm photolysis of H_2O , HOD, and D_2O via the Franck–Condon model, the results are in relatively poor agreement with these experimental trends.

An intriguing alternative possibility is suggested by the work of Brouard and co-workers,⁴ who have studied vibrationally mediated photolysis of HOD in the $4\nu_{\text{OH}}$ and $5\nu_{\text{OH}}$ overtone manifolds. In order to obtain satisfactory agreement with their experimental results for HOD, the Franck–Condon model has been modified to permit additional torque contributions between the recoiling products in the exit channel. This modification is rationalized on the basis of a center-of-mass shift between OD and OH products, which leads to a \approx twofold increase in lever arm for application of exit channel torques for HOD vs H_2O photolysis. This same effect would also be present for D_2O , which would be consistent with the nearly quantitative similarities observed between

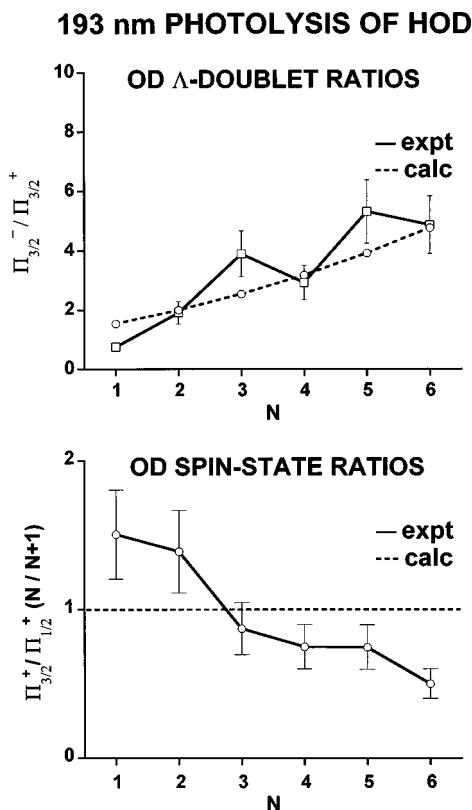


FIG. 6. Λ -doublet ratios of the ${}^2\Pi_{3/2}^+$ and ${}^2\Pi_{3/2}^-$ levels (upper panel) and the spin-state population ratios of the ${}^2\Pi_{3/2}^+$ and ${}^2\Pi_{1/2}^+$ levels (lower panel) as a function of rotational quantum number N for the 193 nm photolysis of HOD. The Λ -doublet ratios predicted for a prompt, planar dissociation are also shown with a dashed line in the top panel. The spin-state ratios are first corrected for state degeneracies with the factor $N/(N+1)$ ($J=N+\frac{1}{2}$ for $\Omega=\frac{3}{2}$ and $J=N-\frac{1}{2}$ for $\Omega=\frac{1}{2}$): a ratio of 1:1, therefore, corresponds to a statistical distribution over the two spin levels.

OD rotational distributions for both D_2O and HOD photolysis systems. Though more theoretical work would be necessary to confirm this picture, these data suggest that exit channel interactions may be non-negligible for D_2O and HOD photolysis at 193 nm.

C. OD Λ -doublet and spin-state population ratios

The population ratios of OD in the Λ -doublet levels (${}^2\Pi_{3/2}^+$ and ${}^2\Pi_{3/2}^-$) and spin-state levels (${}^2\Pi_{3/2}^+$ and ${}^2\Pi_{1/2}^+$) provide additional information about isotopic substitution effects on fragmentation dynamics of water. The experimentally observed Λ -doublet ratios of OD are shown in the top panel of Fig. 6. Also shown with dashed lines are the ratios theoretically predicted for prompt recoil from a planar dissociation geometry. The model explicitly takes into account the N dependence of the Λ -doublet mixing that occurs in the OH-OD products, as described previously for both 157 nm⁵ and 193 nm¹⁰ photolysis of jet-cooled H_2O and D_2O . Although detailed N -dependent structure is undoubtedly present in these curves, the general experimental trend is for an increase in Λ -doublet inversion with rotational quantum number N . Furthermore, the magnitude of this inversion is in

reasonable agreement with the model predictions for a planar dissociation geometry, as also seen in other photolysis studies.

At a more subtle level, the Λ -doublet distributions from HOD are generally more inverted than those from H_2O or D_2O and for several values of N exceed the planar dissociation model predictions. One possible reason for these differences is the influence of the initially prepared rotational states of HOD, H_2O , and D_2O on the dynamics. In photolysis of H_2O at 157 nm,⁵ for example, the initial rotation of H_2O has been shown to greatly diminish the magnitude of Λ -doublet inversion. This is especially dramatic in the limit of room-temperature photolysis of H_2O , where the strong Λ -doublet inversion evident from vibrationally mediated state-selected photolysis essentially vanishes. These rotational averaging effects are significantly reduced for jet-cooled samples, but due to nuclear spin statistics these effects are still present to some degree for H_2O and D_2O . As mentioned above, these species only cool in an expansion into the lowest two rotational 0_{00} and 1_{01} levels, with a 1:3 and 2:1 ratio for H_2O and D_2O , respectively, whereas HOD can cool completely into the 0_{00} ground rotational state. Consequently, the jet-cooled HOD photolysis results reflect less initial state averaging than for either H_2O or D_2O , which may contribute to the slightly more inverted distributions observed experimentally.

As a final comparison, the population ratios in the ${}^2\Pi_{3/2}^+$ and ${}^2\Pi_{1/2}^+$ spin-state levels of OD from HOD are shown in the bottom panel of Fig. 6. The population ratios are corrected by $N/(N+1)$ for differences in state degeneracies to permit direct comparison with the statistical ratio of unity (dashed line). The data indicate a clear trend of decreasing $\Pi_{3/2}^+ / \Pi_{1/2}^+$ spin-state ratios with increasing rotational quantum number N , with substantial deviations ($\pm 50\%$) away from the statistical limit. This trend is convincingly reiterated for H_2O and D_2O as well, indicating that these N -dependent deviations from statistical behavior are a robust feature of the 193 nm photolysis dynamics. It is worth noting that this trend is considerably different from what is observed from 157 nm photolysis studies of H_2O and D_2O in the Franck-Condon region,⁵ where the spin-state distributions are observed to be nearly perfectly in the statistical limit for both OH and OD products. However, it is also relevant that the spin-state distributions at 157 nm were obtained on room-temperature samples, and thus it is not possible to separate effects due to (i) Franck-Condon vs non-Franck-Condon photolysis and (ii) thermal averaging over initial rotational states.

V. DISCUSSION

Quantum scattering calculations have been used to predict branching ratios for photolysis of HOD from a number of vibrational states; in most cases, agreement with the experimental data is quite good. For example, Shafer *et al.*⁵ report an OD/OH ratio of 4 ± 1 for photolysis from ground-state HOD at 157 nm, which is in excellent agreement with the theoretically predicted value¹⁷ of 4.2. Similarly, in vibrationally mediated photolysis studies of $4\nu_{OH}$ HOD at 218.5

nm by Crim and co-workers,³ OD/OH yields are found to be $1 \pm 0.2:1$, which again agree very well with 0.9–1.1 values predicted from theory.³ From simple Franck–Condon arguments, the specificity of this branching ratio is expected to increase dramatically for excitation at lower photolysis energies, which therefore shifts the Condon point on the upper potential surface further into the exit channel region. For example, photolysis studies of $4\nu_{\text{OH}}$ excited HOD at 266 and 240 nm³ result exclusively in OD product formation, with a branching ratio of $>15:1$ for the OD/OH ratio. This again compares favorably with theoretically predicted values of $>10^3:1$ and $>80:1$, respectively, for the two dissociation wavelengths.

However, for other vibrationally mediated photolysis studies of water isotopomers where absolute branching ratios are reported, the agreement is consistently less satisfying. For example, 193 nm photolysis from the ν_{OH} level of HOD leads to a 2.5:1 branching ratio for OH/OD production, which is fourfold smaller than the theoretically predicted ratio¹⁸ of 10:1. Similarly, 193 nm photodissociation studies indicate only a 64(10):1 ratio photolysis cross sections for H₂O vs D₂O,¹⁰ which is more than threefold smaller than the theoretical predictions of $>200:1$ by Schinke and co-workers.⁹ In the current study of ground-state HOD at 193 nm, even larger discrepancies with theory are evident. Specifically, the observed OD/OH branching ratio of 12(8):1 is more than eight times smaller than recent theoretical predictions of $>100:1$.⁹ If one thinks of these branching ratios from one-photon photolysis as the logical extreme of vibrationally mediated photodissociation of molecules with zero-point excitation, theory would appear to be systematically over-predicting the isotope- and/or bond-selectivity of the photodissociation event. Considering that water photolysis currently represents one of the most thoroughly studied ‘‘benchmark’’ systems for truly rigorous tests of polyatomic photodissociation dynamics, these discrepancies are significant and worthy of further investigation.

One feature common to each of these studies is that they involve excitation substantially into the exit channel region, and from a Franck–Condon perspective preferentially sample the classical forbidden ‘‘wings’’ of the lower state vibrational wave function. One possible concern would be that these over-predicted isotope and bond selectivities arise simply from inaccuracies in the upper and lower potential surfaces which would, therefore, be amplified due to errors accumulated in exponentially decreasing regions of the vibrational wave function. Thus, it is important to establish that the theoretical predictions are reasonably insensitive to the choice of potential surface. In our previous study of the photodissociation dynamics of H₂O and D₂O at 193 nm, algorithms developed by Miller and Child¹⁹ were used to calculate the absorption cross-section ratio for these two isotopomers. The approach makes use of semiclassical Wentzel–Kramers–Brillouin (WKB) methods for calculating one-dimensional (1D) overlap matrix elements between lower state bound and excited-state continuum wave functions. Based on the ground-state surface of Sorbie and Murrell⁷ (SM) and excited-state surface of Staemmler and Palma⁸ (SP), this simplified 1D model predicted the H₂O–D₂O

TABLE II. Results of 1D semiclassical model calculations for determining HOD branching ratios at 193 nm. The results are obtained for each ground-state potential surface for the unphotolyzed bond fixed at 0.9710 Å and the HOH–DOD bond angle fixed at 104.52°. The Staemmler and Palma excited-state surface (SP) is used for all calculations. Note that theoretical predictions of the OD–OH ratio are 1 to 2 orders of magnitude larger than experimentally observed. The results previously reported for the absorption cross-section ratios of H₂O and D₂O are included for comparison, which are also overpredicted ($>$ threefold) by theory.

Lower PES	Upper PES	$\sigma_{\text{H-OD}}/\sigma_{\text{D-OH}}$	$\sigma_{\text{H}_2\text{O}}/\sigma_{\text{D}_2\text{O}}^c$
SM ^a	SP ^b –1.0 kcal/mole	139	150
SM ^a	SP ^b	176	203
SM ^a	SP ^b +1.0 kcal/mole	432	244
RW ^c	SP ^b	649	712
Tennyson ^d	SP ^b	6550	7480
Experiment (this work)		12(8)	64(10)

^aReference 7.

^bReference 8.

^cReference 20.

^dReference 21.

^eReference 10.

cross-section ratio to be in nearly quantitative agreement with full 3D scattering calculations of Schinke and co-workers⁹ using these same surfaces. More importantly, the availability of closed form analytical expressions for these matrix elements and photolysis cross-section ratios permits one to evaluate the sensitivity to estimates of theoretical uncertainties in the upper–lower potential surfaces.

A similar theoretical analysis is invoked here to predict (i) the branching ratio for OD/OH formation from 193 nm HOD photolysis and (ii) establish the sensitivity of this branching ratio to uncertainties in the potential surfaces. The details of the approach are described elsewhere;¹⁰ the results of these calculations are summarized in Table II for different ground-state surfaces (Sorbie and Murrell,⁷ Reimers–Watts,²⁰ and Tennyson²¹) and one common upper state surface (Staemmler–Palma⁸). For the widely used Sorbie–Murrell (SM) surface, the calculations predict an HOD photolysis branching ratio for OD–OH formation at 193 nm to be 176:1. This is in good agreement with full 3D scattering calculations and yet overestimates the experimentally observed branching ratio of 12(8):1 by more than an order of magnitude. The experimental and theoretical bond selective cross-section ratios for photolysis of H₂O, HOD, and D₂O are summarized in Fig. 7, with all data sets normalized to the production of OH and H₂O. The propensity for OH cleavage in HOD is only down by roughly twofold from H₂O, which is easily rationalized, since HOD has half of the number of OH bonds as H₂O. However, the level of agreement for cleavage of OD bonds in either D₂O or HOD is significantly worse, with discrepancies of as much as an order of magnitude between theory and experiment.

The robustness of these results to uncertainties in the SM potential have also been tested by repeating the calculations for a uniform ± 1 kcal/mole shift in the SM ground-state potential surface. This reflects a reasonably conservative estimate of the potential surface uncertainties based on the -1 kcal/mole shift necessary to reproduce the photolysis wavelength dependent structure in the UV cross sections for $|04-\rangle$ excited H₂O.²² As listed in Table II, these shifted

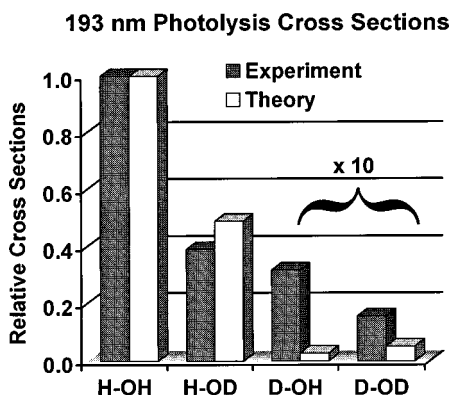


FIG. 7. Sequentially observed and theoretically predicted bond selective UV photolysis cross sections for D_2O and HOD at 193 nm. All values are normalized to H–OH bond cleavage in H_2O , with the two much weaker O–D photolysis channels multiplied by tenfold for ease of visual comparison. The theoretical values are obtained from the 1D semiclassical models described in the text and elsewhere (Refs. 10 and 19).

potential surfaces predict branching ratios of 139:1 and 432:1, respectively, i.e., both more than an order of magnitude too high to bring the theoretically predicted OD/OH branching ratios into agreement with experimental observation. This qualitative trend is also confirmed on the two other H_2O potential surfaces tested, which yield branching ratios as much as two orders of magnitude higher than experimentally observed.

Though the reasons for such striking discrepancies between theory and experiment for such an extensively studied, benchmark photolysis system are not yet fully understood, several possibilities can be suggested. Perhaps the most intriguing of these is that for these extreme non-Franck–Condon excitations, nonadiabatic effects in the different exit channels may begin to be important. As the simplest example, direct excitation to electronic surfaces of higher spin multiplicity could become competitive with far-off resonance absorption from classically forbidden wings in the $\tilde{A} \leftarrow \tilde{X}$ singlet band. Specifically, direct absorption to the lowest triplet state would be significantly red shifted from the $\tilde{A} \leftarrow \tilde{X}$ absorption band, which although quite weak, could begin to play an important role at these long excitation wavelengths and high detection sensitivities ($\approx 10^{-26}$ cm²). Such prospects for *triplet* mediated photolysis dynamics in water are currently being addressed by Schinke and co-workers and will be reported in the accompanying paper.⁹ Of particular interest would be to predict final state distributions from such dynamical channels, and thereby see if triplet state effects could also be contributing to the distinctive rotational, spin-state and/or Λ -doublet distributions experimentally observed from extreme non-Franck–Condon photolysis of HOD, H_2O , and D_2O .

VI. SUMMARY AND CONCLUSIONS

Photolysis distributions and OH–OD yields are obtained for jet-cooled gas isotopic mixtures of H_2O , HOD, and D_2O following far-off-resonance photodissociation at 193 nm. The OD rotational populations indicate strikingly similar and substantially broader distributions for both HOD and D_2O

photolysis than the OH distributions observed for H_2O . The near quantitative agreement between HOD and D_2O results suggests that this is due to a larger lever arm for photorejection of OD vs OH, which amplifies the role of exit channel torques neglected in Franck–Condon models. Furthermore, systematic N -dependent trends in Λ -doublet populations are reiterated in all three isotopomers, consistent with prompt dissociation from a planar geometry. The spin-state distributions also reveal systematic trends common to all three isotopomers, and substantially in contrast with the nearly statistical distributions observed via 157 nm excitation in the Franck–Condon allowed region.

Of specific dynamical interest, analysis of the OD/OH yields as a function of isotopic composition permits relative photolysis cross sections for each of the individual isotopomers to be extracted. The branching ratio for OH vs OD bond cleavage in HOD is determined to be 12(8):1, which qualitatively agrees with the strong isotope effect anticipated for Franck–Condon excitation in the classically forbidden wings of the OH vs OD zero-point vibrational levels. More quantitatively, however, this ratio is over eightfold lower than full 3D quantum scattering predictions obtained by Schinke and co-workers,⁹ which for a prototypical system such as water, represents a major discrepancy between theory and experiment. These branching ratios have also been calculated in a semiclassical 1D model with several other ground-state surfaces as well as for surfaces shifted by ± 1 kcal/mole; the discrepancies are robust with respect to conservative estimates of potential surface uncertainties. These results indicate that the photolysis dynamics of benchmark molecules far from the classically allowed Franck–Condon regime is not yet fully understood and worthy of further theoretical investigation. One intriguing possibility suggested by these studies is that photolysis contributions in the non-Franck–Condon region are occurring from both singlet and triplet potential energy surfaces. Theoretical efforts to explore the influence of multiple surfaces in the photolysis event have been undertaken by Schinke and co-workers,⁹ and will be discussed in the following paper.

ACKNOWLEDGMENTS

This work has been supported by grants from the National Science Foundation. The authors would like to thank Dr. Reinhard Schinke, Dr. Marc Brouard, and Professor Jonathon Tennyson for stimulating discussions.

- ¹I. Bar, Y. Cohen, D. David, T. Arusi-Parpar, S. Rosenwaks, and J. J. Valentini, *J. Phys. Chem.* **95**, 3341 (1991).
- ²S. Hennig, V. Engel, R. Schinke, and V. Staemmler, *Chem. Phys. Lett.* **149**, 455 (1988); V. Engel, V. Staemmler, R. L. Vander Wal, F. F. Crim, R. J. Sension, B. Hudson, P. Andresen, S. Hennig, K. Weide, and R. Schinke, *J. Phys. Chem.* **96**, 3201 (1992).
- ³R. J. Vander Wall, J. L. Scott, F. F. Crim, K. Weide, and R. Schinke, *J. Chem. Phys.* **94**, 3548 (1991); R. L. Vander Wal, J. L. Scott, and F. F. Crim, *ibid.* **92**, 803 (1990).
- ⁴M. Brouard and S. R. Langford, *J. Chem. Phys.* **106**, 6354 (1997).
- ⁵N. Shafer, S. Satyapal, and R. Bersohn, *J. Chem. Phys.* **90**, 6807 (1989); P. Andresen, G. S. Ondrey, B. Titye, and E. W. Rothe, *ibid.* **80**, 2548 (1984).
- ⁶J. Zhang, D. J. Imre, and J. H. Frederick, *Chem. Phys.* **139**, 89 (1989); V. Engel and R. Schinke, *J. Chem. Phys.* **88**, 6831 (1988).

- ⁷K. S. Sorbie and J. N. Murrell, *Mol. Phys.* **29**, 1387 (1975); **31**, 905 (1956).
- ⁸V. Staemmler and A. Palma, *Chem. Phys.* **93**, 63 (1985).
- ⁹T. Schroeder and R. Schinke, *J. Chem. Phys.* **109**, 6641 (1998), following paper.
- ¹⁰D. F. Plusquellic, O. Votava, and D. J. Nesbitt, *J. Chem. Phys.* **107**, 1 (1997).
- ¹¹W. L. Dimpfl and J. L. Kinsey, *J. Quant. Spectrosc. Radiat. Transf.* **21**, 233 (1979).
- ¹²J. W. Pyper, R. S. Newbury, and G. W. Barton, Jr., *J. Chem. Phys.* **46**, 2253 (1967).
- ¹³I. Kirshenbaum, in *Physical Properties and Analysis of Heavy Water*, edited by H. C. Urey and G. M. Murphy (McGraw-Hill, New York, 1951).
- ¹⁴W. A. Van Hook, *J. Phys. Chem.* **76**, 3040 (1972).
- ¹⁵G. G. Balint-Kurti, *J. Phys. Chem.* **84**, 4443 (1986); G. G. Balint-Kurti and M. Shapiro, *Chem. Phys.* **61**, 137 (1981); **72**, 456 (1982).
- ¹⁶R. L. Vander Wal, J. L. Scott, and F. F. Crim, *J. Chem. Phys.* **94**, 1859 (1991); D. Hausler, P. Andersen, and R. Schinke, *ibid.* **87**, 3948 (1987); J. Zhang and D. G. Imre, *ibid.* **90**, 1666 (1989).
- ¹⁷D. J. Imre and J. Zhang, *Chem. Phys.* **139**, 89 (1989).
- ¹⁸J. Zhang, D. G. Imre, and J. H. Frederick, *J. Phys. Chem.* **93**, 1840 (1989).
- ¹⁹M. S. Child, *Semiclassical Mechanics with Molecular Applications* (Clarendon, Oxford, 1991); W. H. Miller, *J. Chem. Phys.* **48**, 464 (1968).
- ²⁰J. R. Reimers and R. O. Watts, *Mol. Phys.* **52**, 357 (1984); D. F. Coker and R. O. Watts, *J. Phys. Chem.* **91**, 2513 (1987); D. F. Coker, R. E. Miller, and R. O. Watts, *J. Chem. Phys.* **82**, 3554 (1985).
- ²¹O. L. Polyansky, P. Jensen, and J. Tennyson, *J. Chem. Phys.* **101**, 7651 (1994).
- ²²K. Weide, S. Hennig, and R. Schinke, *J. Chem. Phys.* **91**, 7630 (1989).